Article

A Refined Reaction-Diffusion Model of Tau-Microtubule Dynamics and Its Application in FDAP Analysis

Maxim Igaev,[1,*] Dennis Janning,[1] Frederik Sündermann,[1] Benedikt Niewidok,[1] Roland Brandt,[1] and Wolfgang Junge[2]
[1]Department of Neurobiology and [2]Department of Biophysics, University of Osnabrück, Osnabrück, Germany

ABSTRACT Fluorescence decay after photoactivation (FDAP) and fluorescence recovery after photobleaching (FRAP) are well established approaches for studying the interaction of the microtubule (MT)-associated protein tau with MTs in neuronal cells. Previous interpretations of FDAP/FRAP data have revealed dwell times of tau on MTs in the range of several seconds. However, this is difficult to reconcile with a dwell time recently measured by single-molecule analysis in neuronal processes that was shorter by two orders of magnitude. Questioning the validity of previously used phenomenological interpretations of FDAP/FRAP data, we have generalized the standard two-state reaction-diffusion equations by 1), accounting for the parallel and discrete arrangement of MTs in cell processes (i.e., homogeneous versus heterogeneous distribution of tau-binding sites); and 2), explicitly considering both active (diffusion upon MTs) and passive (piggybacking upon MTs at rates of slow axonal transport) motion of bound tau. For some idealized cases, analytical solutions were derived. By comparing them with the full numerical solution and Monte Carlo simulations, the respective validity domains were mapped. Interpretation of our FDAP data (from processes of neuronally differentiated PC12 cells) in light of the heterogeneous formalism yielded independent estimates for the association (~2 ms) and dwell (~100 ms) times of tau to/on a single MT rather than in an MT array. The dwell time was shorter by orders of magnitude than that in a previous report where a homogeneous topology of MTs was assumed. We found that the diffusion of bound tau was negligible in vivo, in contrast to an earlier report that tau diffuses along the MT lattice in vitro. Methodologically, our results demonstrate that the heterogeneity of binding sites cannot be ignored when dealing with reaction-diffusion of cytoskeleton-associated proteins. Physiologically, the results reveal the behavior of tau in cellular processes, which is noticeably different from that in vitro.

INTRODUCTION

Biopolymer networks maintain cellular structure, guide intracellular transport, and anchor cellular components. This is of particular importance for neurons where arrays of microtubules (MTs) stabilize the long processes and rail the axoplasmic transport (1). Various MT-associated proteins (MAPs), such as MAP2 and the tau protein, are abundant in neurons, and electron micrographs have provided evidence that they decorate MTs and determine the MT-MT distance in the array (2,3).

The tau protein is highly enriched in the axonal compartment, and one might assume that motor proteins would frequently encounter bound tau along their path (4), which would affect motor-protein-driven axonal transport. In fact, tau was found to reduce the attachment frequency of motor proteins to MTs (5) and to inhibit the motility of kinesin in vitro (6). In stably transfected cultured cells, overexpression of tau inhibited kinesin-dependent trafficking of vesicles (7). However, results from these studies were not consistent with in vivo experiments in squid axoplasm, where even a high (20-fold) excess of tau over its physiological concentration did not influence fast axonal transport processes (8). Analysis of tau knockout or overexpressing mice did not reveal changes in axonal transport rates either, indicating that tau is not required, nor does it adversely affect, axonal transport in the nervous system of living mice (9). Interestingly, in vitro single-molecule imaging experiments provided evidence that MT-stabilizing agents affect the influence of tau on kinesin motility (10), which might explain the differences between in vitro and in vivo studies. Taken together, the data suggest that the tau-MT interaction and regulation of the axonal transport by tau are more complex than previously recognized and require that the spatial arrangement of MTs in axonal arrays be taken into account.

MTs are dynamic polymers, and the dynamic-instability model states that the MT steady state represents a balance between the majority of slowly growing MTs and the minority of rapidly depolymerizing ones (11). In cell-free assays, tau suppresses the steady-state dynamics of MTs already at very low molar ratios of tau to tubulin (12) and influences the mean rate and extent of shortening as well as growing. In addition, tau suppresses catastrophe and increases rescue events, indicating a complex effect on several parameters of the dynamic instability. Consistent with in vitro data, tau

Submitted May 29, 2014, and accepted for publication September 19, 2014.
*Correspondence: maxim.igaev@biologie.uni-osnabrueck.de
Editor: Jose Faraldo-Gomez.

0006-3495/14/12/2567/12 $2.00
http://dx.doi.org/10.1016/j.bpj.2014.09.016

suppresses the MT dynamics and reduces the rate and extent of both growing and shortening events even when microinjected at physiological levels in cultured cells (13). To better understand the role of tau in living cells, it will be relevant to reconcile the tau-MT interaction with its complex effect on the MT dynamics under conditions that prevail in an MT array. Thus, in this work, we focus on the diffusion-reaction of tau in extended processes as opposed to the cell body and the growth cone.

Among live-cell fluorescence microscopy techniques, fluorescence recovery after photobleaching (FRAP (14–16)) and fluorescence decay after photoactivation (FDAP (17)) have been applied previously to study the tau-MT interaction in living cells. The experimental setup and data evaluation are similar in both cases. The molecule of interest is fluorescently tagged, e.g., by some variant of green fluorescent protein (GFP). For FRAP, the molecule of interest is tagged with a GFP; for FDAP, it is tagged with a photoactivatable GFP (PAGFP). A certain region within a cell is irreversibly bleached/photoactivated by a focused laser flash, and the fluorescence intensity distribution as a function of time is monitored in the microscopic region of interest. The recovery/decay transient is fitted by a mathematical model to yield mobility and binding properties of the target molecule. For extracting the parameters of binding and diffusion of tau, the cited authors (14,15,17) made use of phenomenological exponential expressions and approximate solutions to the full reaction-diffusion equations. Whereas the former might prove inadequate when dealing with several diffusing species or reaction-diffusion, the latter need validation through the full numerical solution (18,19). Moreover, the fine structure of MTs in the cellular process (20) was previously ignored. A rigorous treatment of FDAP/FRAP transients requires that the general reaction-diffusion equations be solved. Except in some simplified cases, analytical solutions are usually difficult to obtain. One well-known example is referred to as effective diffusion. John Crank (21) has shown that reaction-diffusion reduces to pseudodiffusion when the binding is nearly instantaneous. The effective diffusion constant is then smaller than the true one by a factor related to the proportion of molecules which are on average free to diffuse. Many biological processes are well interpreted in these terms, e.g., the delayed relaxation of pH pulses along biological membranes (22–24).

The relatively long dwell time of ~4 s of bound tau on MTs, which has been determined from previous FRAP experiments (14,25), seems to conflict with the fact that tau does not interfere with axonal transport and appears incompatible with recent single-molecule data indicating a much more rapid, kiss-and-hop, behavior of tau in axons of living neurons, with a dwell time of ~40 ms on a single MT (26). These discrepancies have prompted us to revisit the kinetics of tau binding using FDAP analysis to determine independently the on- and off-rates of tau in the MT array.

Following the pioneering work on reaction-diffusion of transcription factors in the cell nucleus (18), we develop here differential equations for reaction-diffusion of the tau protein in a cylindrical cellular process, evaluate the full numerical solution, construct analytical solutions under certain simplifying conditions, and check their respective validity domains by comparing them with the full numerical solution and Monte Carlo simulations. The topological fine structure, namely, the arrangement of parallel MT filaments in arrays (20), and the case of diffusing bound tau are further explicitly taken into account. We believe that the interpretation of FDAP transients in light of this theoretical treatment results in new insight on the mechanism and role of the tau-MT interaction in living neuronal cells.

MATERIALS AND METHODS

Construction of expression vectors

Eukaryotic expression plasmids for adult human tau (pRC/CMV-PAGFP-htau(441)) and pRC/CMV-3×PAGFP have been described previously (27,28).

Cell culture and transfection

PC12 cells were cultured in serum-DMEM essentially as previously described (29). Undifferentiated cells were plated on 35-mm polylysine and collagen-coated glass-bottom culture dishes (MatTek, Ashland, MA) at 10^4 cells/cm^2. Transfection was performed in Opti-MEM (Gibco, Langley, OK) with Lipofectamin 2000 (Invitrogen, Carlsbad, CA) as reported previously (27). For neuronal differentiation, medium was exchanged against DMEM with 1% (vol/vol) serum containing 100 ng/mL 7S mouse NGF (Alomone Laboratories, Jerusalem, Israel), and the culturing was continued for 4 days, with one medium exchange after 2 days. Before imaging, the medium was exchanged against the same medium containing DMEM without phenol red.

Confocal microscopy

Live imaging was performed on a laser scanning microscope (Eclipse TE2000-U inverted; Nikon, Tokyo, Japan) equipped with argon (488 nm), helium/neon (543 nm), and blue diode (405 nm) lasers. A Fluor 60× (NA 1.4) UV-corrected objective lens was used for photoactivation. The microscope was enclosed in an incubation chamber maintained at 37°C and 5% CO_2 (Solent Scientific, Fareham, United Kingdom). Automated image acquisition after photoactivation was carried out as previously described (17). A single iteration of the photoactivation pulse employed the blue diode. It was performed using rectangular photoactivation regions with lengths of 16 μm and 8 μm for 3×PAGFP and PAGFP-tau, respectively, and lasted 30–60 ms depending on the photoactivation region size. Frames were obtained at a frequency of 1 frame/s, and 112 frames were collected per experiment. Standard series were collected at resolution of 256 × 256 pixels.

RESULTS

Model outline

The process of a neuronal cell is modeled as an infinite cylinder filled with binding sites for the protein of interest

(e.g., tau), whereby one of the coordinate axes, say Oz, is aligned with the cellular process. The binding equilibrium of this protein, TF (at concentration [TF] when free), with binding sites, MT (at concentration [MT]), in the cylinder is as follows:

$$\mathrm{TF} + \mathrm{MT} \underset{k_{\mathrm{off}}}{\overset{k_{\mathrm{on}}}{\rightleftharpoons}} \mathrm{TB}, \tag{1}$$

where TB denotes bound molecules at concentrations [TB], and k_{on} ($\mathrm{M}^{-1}\ \mathrm{s}^{-1}$) and k_{off} (s^{-1}) are the on- and off-rate constants, respectively. In this section, a rigorous reaction-diffusion theory is developed on the basis of seven assumptions. For the sake of clarity, the validity of these assumptions and how violations could affect the results of this study are postponed to the Discussion section.

1. The PAGFP tag has no effect on the tau-MT interaction.
2. Binding properties of tau to MTs are independent of the longitudinal position within the cellular process on spatial scales of FDAP/FRAP, i.e., $k_{\mathrm{on}} \neq f(z)$ and $k_{\mathrm{off}} \neq f(z)$, where $f(z)$ is an arbitrary function of z.
3. Before the photoactivating laser flash is fired, the protein ensemble has attained equilibrium with the MT network and the equilibrium concentrations $[\mathrm{TF}]_{\mathrm{eq}}$, $[\mathrm{MT}]_{\mathrm{eq}}$, and $[\mathrm{TB}]_{\mathrm{eq}}$ have been settled.
4. Photoactivation does not disturb the number of the binding sites but only the fraction of detectable molecules, independent whether free or bound ($[\mathrm{MT}] = [\mathrm{MT}]_{\mathrm{eq}} = \mathrm{const}$).
5. Transport of tau along the cellular process can be neglected during a FDAP/FRAP experiment.
6. The concentration of specific binding sites related to MTs is large relative to that of other binding sites unrelated to MTs.
7. The total concentration of tau molecules does not considerably exceed the concentration of the available binding sites ($[\mathrm{TF}]_{\mathrm{eq}} + [\mathrm{TB}]_{\mathrm{eq}} \leq [\mathrm{MT}]_{\mathrm{eq}}$).

Note that the dependence of k_{on} and k_{off} on the transversal coordinates x and y (heterogeneous tau-binding sites), as well as the case when bound tau molecules diffuse upon MTs, will be further explicitly considered. So far, the resulting reaction-diffusion equations read as follows:

$$\frac{\partial[\mathrm{TF}]}{\partial t} = D\nabla^2[\mathrm{TF}] - k^*_{\mathrm{on}}[\mathrm{TF}] + k_{\mathrm{off}}[\mathrm{TB}], \tag{2A}$$

$$\frac{\partial[\mathrm{TB}]}{\partial t} = k^*_{\mathrm{on}}[\mathrm{TF}] - k_{\mathrm{off}}[\mathrm{TB}], \tag{2B}$$

where $k^*_{\mathrm{on}} = k_{\mathrm{on}}[\mathrm{MT}]_{\mathrm{eq}}$ (s^{-1}) is the pseudo-first-order on-rate and ∇ is the cylindrical nabla operator. Normalization of the free and bound equilibrium concentrations by the total concentration $[\mathrm{T}]_{\mathrm{tot}} = [\mathrm{TF}]_{\mathrm{eq}} + [\mathrm{TB}]_{\mathrm{eq}}$ results in

$$[\mathrm{TB}]_{\mathrm{eq}} = \frac{k^*_{\mathrm{on}}}{k_{\mathrm{off}}}[\mathrm{TF}]_{\mathrm{eq}} = \frac{k^*_{\mathrm{on}}/k_{\mathrm{off}}}{1 + k^*_{\mathrm{on}}/k_{\mathrm{off}}}. \tag{3}$$

We derive solutions to Eq. 2 for the case of a cylinder of radius R and infinite length. In our experiments, we chose cells with straight processes >30 μm in length so that neither the tip of the process nor the cell body influenced the fluorescence distribution during the observation time. A cylindrical photoactivation region with sharp axial borders serves as a good idealization to the photoactivation profile, as validated by subsidiary numerical simulations (see Supporting Material). Regarding the angle and radial properties of the photoactivation profile, we presume that these are uniform independently of the angle and the radial distance from the axial line of the process, since the width of the photoactivation rectangle in the experimental set-up was chosen to be larger than the apparent thickness (due to diffraction) of cellular processes (~2 μm). Thus, the angular and radial terms in Eq. 2 vanish and only the axial component $D\partial^2[\mathrm{TF}]/\partial z^2$ remains.

Simplified solutions

In the Supporting Material, we provide a complete procedure for obtaining the general solution to Eq. 2 for the FDAP decay within a cylindrical activation region. The Laplace image of the normalized fluorescence intensity averaged over the photoactivation region is

$$\overline{\mathrm{FDAP}}(p) = \frac{[\mathrm{TF}]_{\mathrm{eq}}}{p}\left(1 - \frac{1 - \exp(-2q\sigma)}{2q\sigma}\right)\left(1 + \frac{k^*_{\mathrm{on}}}{p + k_{\mathrm{off}}}\right) + \frac{[\mathrm{TB}]_{\mathrm{eq}}}{p + k_{\mathrm{off}}}, \tag{4}$$

where p is the inverse time, σ is the half-length of the activation region, and q is a parameter that depends on p, k^*_{on}, k_{off}, and D (see Supporting Material). Inversion of the Laplace image yields the expected time course of the FDAP signal. The inversion can always be numerically achieved (see Supporting Material). Imposing restrictions on the parametric set in Eq. 4, we find simplified solutions in four special cases (see Supporting Material for details on the derivation). Here, we adhere to the classification introduced by McNally and colleagues (18,19). The four special cases have the following names and properties.

Pure diffusion

Most of PAGFP-tagged molecules are free and infrequently interact with the MT network.

Effective diffusion

The reaction process is much faster than diffusion. The binding equilibrium is rapidly established.

Reaction dominant

Diffusion is much faster than the reaction process. Dissociation of PAGFP-tagged molecules from the MT binding sites strongly regulates the relaxation of the FDAP signal.

Hybrid behavior

The majority of the molecules are bound. Diffusion and binding have similar timescales.

FDAP experiments on tau diffusion in cellular processes of neuronal cells have been previously interpreted only in terms of effective diffusion and the reaction-dominant case (see, e.g., Konzack et al. (14) and Weissmann et al. (17)), and by phenomenological multiexponential fits (15). Table 1 lists the above-mentioned simplified solutions correlated with the corresponding FDAP(t) or the Laplace transforms and conditions at which these are achieved. The respective parametric areas where the four simplified solutions are fair approximations to the full numerical solution are shown in Fig. 1 (see also Supporting Material and Fig. S1).

Diffusing-bound-state model

It has been assumed hitherto that only free tau diffuses, whereas bound tau is immobile. Here, this particular restriction is dropped. When bound molecules also diffuse, the reaction-diffusion equations read as follows:

$$\frac{\partial[\mathrm{TF}]}{\partial t} = D_\mathrm{F}\nabla^2[\mathrm{TF}] - k^*_\mathrm{on}[\mathrm{TF}] + k_\mathrm{off}[\mathrm{TB}], \qquad (5\mathrm{A})$$

$$\frac{\partial[\mathrm{TB}]}{\partial t} = D_\mathrm{B}\nabla^2[\mathrm{TB}] + k^*_\mathrm{on}[\mathrm{TF}] - k_\mathrm{off}[\mathrm{TB}], \qquad (5\mathrm{B})$$

where it is presumed that $D_\mathrm{B} < D_\mathrm{F}$. Following the same solution strategy as for Eq. 2, the Laplace image of the normalized fluorescence intensity, when averaged over the photoactivation region, is

$$\overline{\mathrm{FDAP}}(p) = \frac{1}{p} - A(p)\frac{1-\exp(-2\lambda_1\sigma)}{2\lambda_1\sigma} + B(p)\frac{1-\exp(-2\lambda_2\sigma)}{2\lambda_2\sigma}, \qquad (6)$$

where p is again the inverse time, σ is the half-length of the activation region, and $A(p)$, $B(p)$, and $\lambda_{1,2}$ are parameters that depend on p, k^*_on, k_off, and D_F and D_B (see Supporting Material). Analysis of the parametric space is represented in Fig. S2.

The refined model

The models in Eqs. 2 and 5 describe reaction-diffusion of an MT-associated protein in a cylinder with homogeneously distributed binding sites. Any fine structure, e.g., the packing of equally spaced, parallel MTs in a cellular process (20), is ignored (Fig. 2, *left*). The resulting parameters k^*_on, k_off, and D are hence merely phenomenological and do not reflect the dynamics of diffusion between and binding to single MTs in the array. In previous studies on the macroscopic diffusion of molecules in a fiber biopolymer network (30,31), two further parameters were introduced, namely, the volume fill factor of the network and its orientation. In the following, we model the reaction-diffusion of molecules in an infinite cylinder of radius R filled with an array of N_MT equally spaced (inter-MT distance $R_\mathrm{MT\text{-}MT}$) and parallel MTs, each of radius R_MT (Fig. 2, *middle*). It is assumed that the diffusion of tau molecules is restricted to the cytosolic phase between MTs and that bound molecules do not diffuse. The parallel orientation of MTs in the cylinder makes it possible to divide this problem into two: reaction-diffusion in the transverse plane and longitudinal diffusion. Let us start with the former.

Given the concentration of free molecules, [TF], the concentration of binding sites, [MT], and the concentration of bound molecules in the MT phase, [TB], the system of

TABLE 1 Theoretical FDAPs for the four simplified solutions and parametric areas of their validity

Name	*FDAP*(t)	Condition
Pure diffusion	$\mathrm{FDAP}_\mathrm{pure}(t) = erf\sqrt{\frac{\tau_D}{t}} + \sqrt{\frac{t}{\pi\tau_D}}\left(\exp\left(-\frac{\tau_D}{t}\right) - 1\right),\ \tau_D = \sigma^2/D$	$k^*_{on} << k_{off}$
Effective diffusion	$\mathrm{FDAP}_\mathrm{eff}(t) = erf\sqrt{\frac{\tau_\mathrm{eff}}{t}} + \sqrt{\frac{t}{\pi\tau_\mathrm{eff}}}\left(\exp\left(-\frac{\tau_\mathrm{eff}}{t}\right) - 1\right),\ \tau_\mathrm{eff} = \tau_D(1 + k^*_\mathrm{on}/k_\mathrm{off})$	$\tau_D >> 1/k^*_{on}$
Reaction dominant*	$\mathrm{FDAP}_\mathrm{reaction}(t) = [\mathrm{TF}]_\mathrm{eq}\mathrm{FDAP}_\mathrm{pure}(t) + [\mathrm{TB}]_\mathrm{eq}\exp(-k_\mathrm{off}t)$	$\tau_D << 1/k^*_{on}$
Hybrid behavior	$\overline{\mathrm{FDAP}}_\mathrm{hybrid}(p) = \frac{1}{p + k_\mathrm{off}}\left(\frac{k_\mathrm{off}}{p}\left(1 - \frac{1-\exp(-2q\sigma)}{2q\sigma}\right) + 1\right)$	$k^*_{on} >> k_{off}$ $\tau_D \sim 1/k^*_{on}$

*Note that the reaction-dominant approximation is defined here according to Michaelman-Ribeiro et al. (19), where a similar formalism was introduced for fluorescence correlation spectroscopy analysis, unlike in the original definition for FRAP (18).

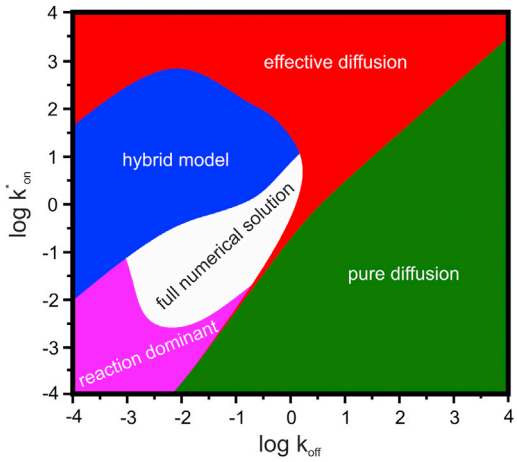

FIGURE 1 Superposition of the validity areas of the four simplified solutions. The regime space shows where each simplified solution approximates well the full numerical solution (the sum of squared residuals, res^2, is <0.01, $D = 10\ \mu m^2/s$, $\sigma = 2\ \mu m$). The area where none of the simplified solutions is suitable is assigned to the full numerical solution. While constructing the superposition, overlaps between different validity areas were assigned to the one for the simplified solution with the fewest number of fit parameters. To see this figure in color, go online.

equations describing lateral reaction-diffusion in the most general case is

$$\frac{\partial[\mathrm{TF}]}{\partial t} = \nabla_\perp \cdot D^\perp(\mathbf{r}_\perp)\nabla_\perp[\mathrm{TF}] + R_\mathrm{F}(\mathbf{c}, \mathbf{r}_\perp), \tag{7A}$$

$$\frac{\partial[\mathrm{MT}]}{\partial t} = R_\mathrm{MT}(\mathbf{c}, \mathbf{r}_\perp), \tag{7B}$$

$$\frac{\partial[\mathrm{TB}]}{\partial t} = R_\mathrm{B}(\mathbf{c}, \mathbf{r}_\perp), \tag{7C}$$

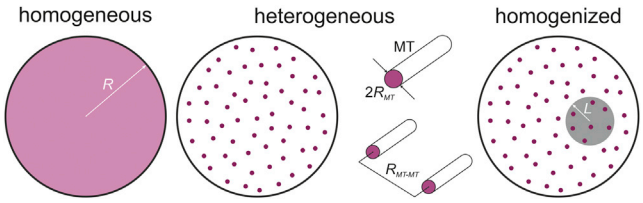

FIGURE 2 Homogeneous and heterogeneous distributions of binding sites over the cross section of the cellular process. (*Left*) In the homogeneous model, tau molecules diffuse and can bind at every position in the cellular process. (*Middle*) If the fine structure of MT packing in the cellular process is explicitly considered, tau molecules diffuse in cytosol and interact with binding sites that are concentrated on MT filaments. The average MT-MT distance ($R_{\mathrm{MT\text{-}MT}}$) in processes of PC12 cells significantly exceeds the size of each MT filament (R_MT). (*Right*) The effective medium approach (EMA) properly homogenizes the heterogeneous model on scales $R_\mathrm{MT} << L << R$ (*gray circle*), thus implicitly accounting for the fine MT structure, in contrast to a simple assumption that the binding sites are smoothed over the volume of the process (*left*). To see this figure in color, go online.

where $\mathbf{c} = ([\mathrm{TF}], [\mathrm{MT}], [\mathrm{TB}])$ is a vector composed of the concentrations, $\mathbf{r}_\perp$ a position vector in the transversal plane, and $\nabla_\perp$ the 2D nabla operator represented in a polar coordinate system. The diffusion constant of the free-molecule fraction, $D^\perp(\mathbf{r}_\perp)$, and the nonlinear reaction rates, R_i, where $i = \mathrm{F}, \mathrm{MT}, \mathrm{B}$, are expressed as

$$D^\perp(\mathbf{r}_\perp) = D(1 - \theta(\mathbf{r}_\perp)), \tag{8A}$$

$$\begin{aligned} R_\mathrm{F}(\mathbf{c}, \mathbf{r}_\perp) &= R_\mathrm{MT}(\mathbf{c}, \mathbf{r}_\perp) = -R_\mathrm{B}(\mathbf{c}, \mathbf{r}_\perp) \\ &= \sum_k \big(-\overline{k}_\mathrm{on}[\mathrm{TF}][\mathrm{MT}] + \overline{k}_\mathrm{off}[\mathrm{TB}] \big)\theta(\mathbf{r}_\perp), \end{aligned} \tag{8B}$$

where $\theta(\mathbf{r}_\perp) = 1$ only within the MT phase and zero elsewhere, and $\overline{k}_\mathrm{on}$ and $\overline{k}_\mathrm{off}$, are the on- and off-rate constants, respectively. To our knowledge, there is no analytical solution to Eq. 7. There have been several studies (32–35) suggesting mathematical methods to homogenize strongly heterogeneous systems of reaction-diffusion equations by means of coarse-grain averaging. One such method is the effective medium approach (EMA) (34,35). The idea behind it is to replace the heterogeneous system in Eq. 7 with an effective one that describes the reaction-diffusion on an intermediate spatial scale between the size of the reactive obstacle and that of the total system (Fig. 2, *right*). The desired system is expected to take the form

$$\frac{\partial\langle[\mathrm{TF}]\rangle}{\partial t} = D^\perp_\mathrm{eff}(\varphi)\nabla^2_\perp\langle[\mathrm{TF}]\rangle + R^\mathrm{eff}_\mathrm{F}(\langle\mathbf{c}\rangle, \varphi), \tag{9A}$$

$$\frac{\partial\langle[\mathrm{MT}]\rangle}{\partial t} = R^\mathrm{eff}_\mathrm{MT}(\langle\mathbf{c}\rangle, \varphi), \tag{9B}$$

$$\frac{\partial\langle[\mathrm{TB}]\rangle}{\partial t} = R^\mathrm{eff}_\mathrm{B}(\langle\mathbf{c}\rangle, \varphi), \tag{9C}$$

where $D^\perp{}_\mathrm{eff}$ and R_i^eff are the effective diffusion coefficient and the effective nonlinear reaction rates, respectively, and φ is the volume fill factor of MTs. The angled brackets represent the coarse-grain average over the intermediate scale. The effective medium approach (35) then yields the effective diffusion coefficient and the effective reaction rates given by

$$D^\perp_\mathrm{eff}(\varphi) = D(1 - 2\varphi), \tag{10A}$$

$$R^\mathrm{eff}_\mathrm{F} = R^\mathrm{eff}_\mathrm{MT} = -R^\mathrm{eff}_\mathrm{B} = -\varphi\overline{k}_\mathrm{on}\langle[TF]\rangle\langle[MT]\rangle + \varphi\overline{k}_\mathrm{off}\langle[TB]\rangle. \tag{10B}$$

To further account for the longitudinal diffusion, a diffusive term $D\partial^2[TF]/\partial z^2$ is added to Eq. 9A. We assume in doing so that the diffusion along the cylindrical axis is less sensitive to restrictions brought in by the MT network. It was not a priori evident that the longitudinal diffusion is not affected by the parallel MTs. Monte Carlo simulation of diffusion

in a cylinder filled with MTs at different volume fill factors showed that it holds true (Fig. 3).

Finally, making the same assumptions (1–7) as for the homogeneous case, the resulting effective 3D system becomes

$$\frac{\partial\langle[\mathrm{TF}]\rangle}{\partial t} = D\frac{\partial^2\langle[\mathrm{TF}]\rangle}{\partial z^2} - k^*_{\mathrm{on}}\langle[\mathrm{TF}]\rangle + k_{\mathrm{off}}\langle[\mathrm{TB}]\rangle, \quad (11\mathrm{A})$$

$$\frac{\partial\langle[\mathrm{TB}]\rangle}{\partial t} = k^*_{\mathrm{on}}\langle[\mathrm{TF}]\rangle - k_{\mathrm{off}}\langle[\mathrm{TB}]\rangle, \quad (11\mathrm{B})$$

where $k^*_{\mathrm{on}} = \varphi\overline{k}_{\mathrm{on}}[\mathrm{MT}]_{\mathrm{eq}}$ and $k_{\mathrm{off}} = \varphi\overline{k}_{\mathrm{off}}$ denote the apparent rate constants. The structure of Eq. 11 entirely replicates that of Eq. 2, except that both actual reaction rates, $\overline{k}_{\mathrm{on}}$ and $\overline{k}_{\mathrm{off}}$, are now likewise $1/\varphi$ times increased compared to the homogeneous ones. It should also be noted that the equilibrium constant of tau binding to MTs is not affected by EMA, i.e., $K_{\mathrm{eq}} = k_{\mathrm{on}}/k_{\mathrm{off}} = \overline{k}_{\mathrm{on}}/\overline{k}_{\mathrm{off}}$.

FDAP fitting and error analysis

Analysis of FDAP data was performed by a self-written routine (see Supporting Material). After performing photoactivation, the average of several FDAP curves, $f(t_i)$, was calculated together with the standard deviation at each time point, t_i ($\sigma(t_i)$) The averaged curve was fit to the full reaction-diffusion models, Eqs. 2 and 5, as well as to each of the simplified solutions (see Table 1). The script minimized the χ^2-value, defined as $\chi^2 = \sum_i[(f(t_i) - \mathrm{FDAP}(t_i))/\sigma_i]^2$, where FDAP($t$) represents the fitted function. Errors for estimated parameters were calculated as described in the Supporting Material and included dispersion of the experimental data.

To decide which model/approximation better described the experimental FDAP signal, the reduced ${\chi_\nu}^2 = \chi^2/(n - n_p - 1)$ values, where n is the number of time steps, and n_p is the number of fit parameters, were compared for models with the same number of fit parameters. For those that had a different number of fit parameters, we used F-tests at the 95% confidence level for the reduced ${\chi_\nu}^2 = \chi^2/(n - n_p - 1)$.

Tau binding and diffusion in processes of living PC12 cells studied by the homogeneous model

In line with the previous work (17), FDAP experiments with a triple-PAGFP (3×PAGFP) were carried out as a control for the case of pure diffusion without binding. The molecular mass of 3×PAGFP is similar to that of PAGFP-tau (82.8 kDa for 3×PAGFP and 75.2 kDa for PAGFP-tau). Fig. 4 *A* shows the observed, averaged time course of the FDAP signal and Fig. 4 *B* the fit by the pure-diffusion approximation. The fit revealed the diffusion constant $D = 13.9 \pm 2.4$ μm^2/s for 3×PAGFP. Moving forward to FDAP experiments with PAGFP-tau, we assumed to reduce the number of fit parameters that its diffusion coefficient (recalculated according to the mass dependence, $D \sim M^{-1/3}$, and taken as 14.4 μm^2/s) was approximately the same as that for 3×PAGFP. This value was in good correspondence with the theoretically expected value (14).

Fig. 5 shows the average time course of the FDAP signal for PAGFP-tau (Fig. 5 *A*) and various fits to this curve (Fig. 5, *B* and *C*). The decay was much slower than that observed for 3×PAGFP. This is compatible with the expected

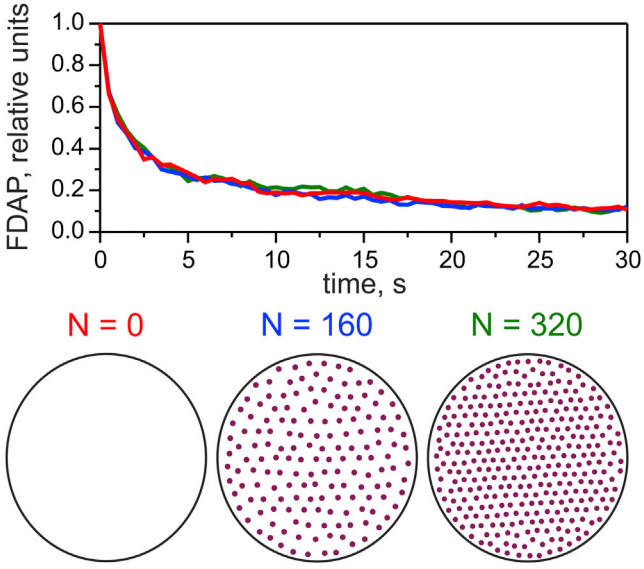

FIGURE 3 Monte Carlo simulations of FDAP transients for a nonreactive molecule diffusing through the MT network along the cellular process at various densities of MT packing. The FDAP transients were computed as described in the Supporting Material ($D = 3$ μm^2/s, $\sigma = 2$ μm). The decays were unaffected by the density of MT packing (i.e., the volume fill factor), which was chosen to be less than the percolation threshold ($\varphi = 0.5$) for transversal diffusion (see Eq. 10A). To see this figure in color, go online.

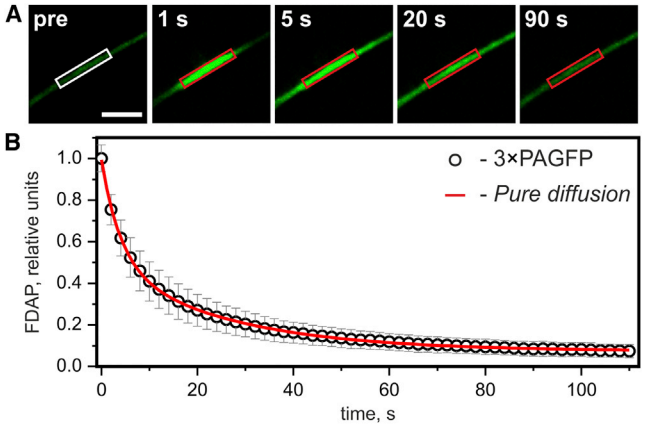

FIGURE 4 FDAP of 3×PAGFP in cellular processes of PC12 cells. (*A*) A confocal image series of a PC12 cell transfected to express 3×PAGFP. The photoactivation region (with half-length $\sigma = 8$ μm) was located in the middle of cellular processes. Scale bar, 10 μm. (*B*) The experimental FDAP transient (*black circles*, mean ± SD, $n = 38$) was well fitted by the pure-diffusion approximation (*red curve*; see Table 1), yielding $D = 13.9 \pm 2.4$ μm^2/s (estimate ± fit error). To see this figure in color, go online.

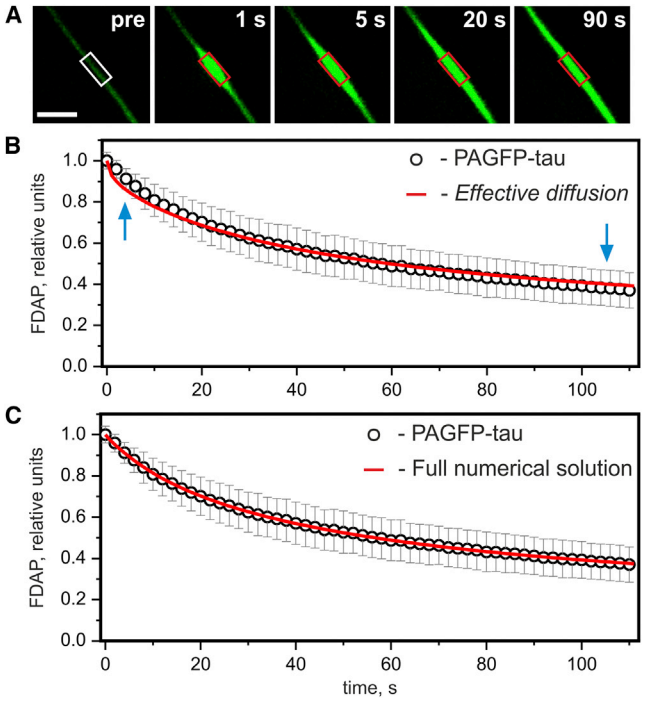

FIGURE 5 FDAP of PAGFP-tau in processes of PC12 cells. (*A*) A confocal image series of a PC12 cell transfected to express PAGFP-tau. Photoactivation was performed in the middle of the cellular process (with the half-length $\sigma = 4$ μm). Scale bar, 10 μm. (*B*) The experimental FDAP for PAGFP-tau (*black circles*, mean ± SD, $n = 38$) is slowed down by transient interactions of tau molecules with MTs, as expected. In contrast to 3×PAGFP, the experimental FDAP transient for PAGFP-tau is not well fitted by either pure or effective diffusion (see Table 1). Blue arrows indicate discrepancies between the fit and the experimental FDAP transient. (*C*) The full numerical solution yields a better fit ($k^*_{on} = 6.2 \pm 3.2$ s^{-1}, $k_{off} = 0.13 \pm 0.06$ s^{-1}, estimate ± fit error) compared to pure and effective diffusion, as ensured by the F-test. The full spectrum of estimates provided by the full numerical solution and the four simplified solutions is given in Table 2. To see this figure in color, go online.

reduction of the FDAP decay due to transient binding of tau to MTs. We found that fits by the pure- and effective-diffusion models were nonoptimal ($\chi_\nu^2 = 11.1$; see Fig. 5 *B*). The fit by the full numerical solution provided much better coincidence with the experimental curve ($\chi_\nu^2 = 0.22$ (Fig. 5 *C*)). Here, the reduced χ_ν^2-value was by a factor of ~50 smaller than that provided by the fit with the pure- and effective-diffusion models. The statistical F-test confirmed this observation. We then asked whether any of the other two simplified solutions produces good fits to the experimental FDAP for PAGFP-tau. Only the hybrid behavior did ($\chi_\nu^2 = 0.19$). Table 2 summarizes the resulting fit parameters, the fractions of bound molecules, and χ_ν^2-values provided by each of the simplified regimes and the full numerical solution.

The estimated on- and off-rates suggest a rather long dwell time of PAGFP-tau on MTs, namely, $\tau_{dwell} = 1/k_{off} \approx 7.7$ s and an association time $\tau_{assoc} = 1/k^*_{on} \approx 0.16$ s (based on the full numerical solution). The pseudoequilibrium constant, $K^*_{eq} = k^*_{on}/k_{off} \approx 48$, was high and corresponded to ~98% of the total PAGFP-tau population being bound to MTs on average over time (see Eq. 3). The long (apparent) dwell time is compatible with a previous study (14) where the effective-diffusion and reaction-dominant approximations were employed on an ad hoc basis.

TABLE 2 Estimated parameters with errors obtained from fits by the full numerical and four simplified solutions

Name	Estimated parameters	Fraction of bound molecules, $[TB]_{eq}$, %	χ_ν^2-value
Full numerical solution	$k^*_{on} = 6.2 \pm 3.2$ s^{-1} $k_{off} = 0.13 \pm 0.06$ s^{-1}	98.0	0.22
Pure diffusion*	$D = 0.25 \pm 0.10$ μm^2/s	—	11.1
Effective diffusion	$D_{eff} = 0.25 \pm 0.10$ μm^2/s $k^*_{on}/k_{off} = 56.6 \pm 15.1$	98.3	11.1
Reaction dominant	$k^*_{on} = 0.06 \pm 0.03$ s^{-1} $k_{off} = 0.009 \pm 0.003$ s^{-1}	86.3	18.1
Hybrid behavior	$k^*_{on} = 6.6 \pm 4.0$ s^{-1} $k_{off} = 0.13 \pm 0.07$ s^{-1}	98.1	0.19

*As follows from Table 1, the pure and effective diffusion approximations are structurally identical and provide only one fit parameter. However, if the free diffusion constant is known, one can calculate the ratio k^*_{on}/k_{off}. The estimated values for the diffusion constant and reaction rates are given as estimate ± fit error. The fraction of bound molecules was calculated according to Eq. 3.

Invoking the diffusion of bound tau

A previous study (36) (see also Scholz and Mandelkow (25)) suggested that tau might diffuse along the MT lattice in vitro with a diffusion constant of ~0.3 μm^2/s. We found that the full numerical solution for the diffusing-bound-state model (Eq. 5) provided a good fit to the experimental curve for PAGFP-tau ($\chi_\nu^2 = 0.3$). However, it held only when the diffusion constant for the bound state (D_B) converged to zero. At nonzero values of D_B, the fitting yielded much greater χ_ν^2. The estimates for the on- and off-rates were compatible with those revealed by the model without bound diffusion (see, *Full numerical solution* and *Hybrid behavior*), namely, $k^*_{on} = 7.9 \pm 3.9$ s^{-1} and $k_{off} = 0.16 \pm 0.07$ s^{-1}. Using the statistical F-test to compare the fits by the full numerical solutions of Eqs. 2 and 5 showed no significant difference. We hence conclude that diffusion of tau in the bound state, even if it exists, is negligible.

Invoking the heterogeneous distribution of binding sites in the MT array

The long (apparent) dwell time of tau on MTs has resulted from a reaction-diffusion model with a homogeneous distribution of tau-binding sites in a cylindrical volume. What if the heterogeneous distribution of binding sites in the array of parallel MTs is taken into account? According to the refined kinetic model (Eq. 11) the apparent on- and off-rates

differ from the actual ones by the volume fill factor of MTs in the cellular process. The actual association and dwell times are φ-times shorter than the apparent ones, namely, $\overline{\tau}_{\mathrm{assoc}} = 1/\overline{k}^{*}_{\mathrm{on}} = \varphi\tau_{\mathrm{assoc}}$ and $\overline{\tau}_{\mathrm{dwell}} = 1/\overline{k}_{\mathrm{off}} = \varphi\tau_{\mathrm{dwell}}$. The upper bound of the volume fill factor for the given topology of MTs (Fig. 2, *middle*) was estimated as $\varphi_{\mathrm{max}} \approx 0.013$ (see Supporting Material). Recalculation of the values for the actual association and dwell times for PAGFP-tau yields ~2 ms and ~100 ms, respectively. The estimates are based on the hybrid-behavior approximation.

There are, however, two possible reasons for overestimating the interaction times. First, the volume fill factor is difficult to assess precisely. The MT-MT distance in processes of PC12 cells can vary and is in fact 70 $\pm$ 20 nm (20), whereas for the calculation of φ_{max}, optimal packing of MTs in the cellular process with a round cross section was assumed. In addition, the shape of the cross section of the process and the number of MTs in the array may differ from those reported by Jacobs and Stevens (20), leading to an even more reduced φ. Thus, both $\overline{\tau}_{\mathrm{assoc}}$ and $\overline{\tau}_{\mathrm{dwell}}$ may be equally overestimated. Second, anomalous free diffusion of PAGFP-tau in processes of living neuronal cells due to obstacles other than MTs also might influence the macroscopic dynamics. These obstacles have no orientation (in contrast to MTs) and are randomly distributed in the cellular processes, thus contributing to the hindered macroscopic diffusion of proteins in cytosol. As previously shown by Monte Carlo simulations (37), kinetic models that ignore the diffusion hindrance brought in by nonreactive obstacles may overestimate the dwell time of the molecules under study for large photoactivation/bleach areas (≥ 2 μm).

DISCUSSION

Elucidations of model assumptions

In this section, we elucidate some of the simplifying assumptions regarding the reaction-diffusion model in Eq. 2 as introduced in the Results section and discuss possible violations.

1. The PAGFP tag has no effect on the protein-MT interaction. It is known that the carboxy-terminal half of tau contains three or four imperfect repeats, which are involved in MT binding (38,39). To minimize potential interference with its MT interaction, PAGFP was fused to the N-terminus of tau. Although tau is an intrinsically unstructured protein, the possibility that modifying the N-terminus may affect the behavior of tau cannot be completely excluded. However, since there are no clear experimental data that would suggest a dramatic effect of the amino-terminal tag on the function of tau, we consider the assumption to be appropriate.
2. Properties of tau binding to MTs are independent of the longitudinal position within the cellular process on spatial scales of FDAP/FRAP. It has been shown that there is a gradient of tau within the axon, namely, that the concentration of tau gradually increases toward the growth cone (40,41). Although the basis of this is still not clear, one can speculate on possible mechanisms. First, the gradient might arise due the fact that tau is actively transported toward the growth cone (25). However, in the elucidation to assumption 5 (see below), we show that this does not affect the modeling. Second, the gradient might arise due to differences in the affinity of tau for MTs along the cellular process, i.e., when $k_{\mathrm{on}} = f(z)$ and $k_{\mathrm{off}} = f(z)$, where $f(z)$ is an arbitrary function of z. If this is true, it could explain the approximately threefold increase of fluorescence intensity in axons over a distance of several hundreds of micrometers toward the growth cone (see Fig. 6 in Black et al. (40)). Nevertheless, on the spatial scale of an FDAP/FRAP experiment (tens of micrometers), the variation of the gradient in the middle of axons is too weak. Thus, we can assume k_{on} and k_{off} of tau to be independent of the position along the cellular process. In addition, we used the PC12 cell system, where this gradient may not occur at all.
3. Before the photoactivating laser flash is fired, the protein ensemble has attained equilibrium with the MT network. Most FDAP/FRAP measurements are performed on a timescale of minutes, whereas protein expression lasts for hours. In the case of tau, a newly expressed protein also has to thread through the complex MT network to get from the cell body to cellular processes; its apparent mobility is reduced by infrequent interactions with MTs. It was suggested recently that tau can be translocated into axons via transport of tau mRNAs that are translated there, hence creating local sources of tau (25,42). This mechanism appears realistic, but again on timescales much longer than the 112 s of our FDAP experiments. In addition, the FDAP method is not capable of tracing freshly made proteins. Once the laser flash has been fired, only the activated population is monitored. Thus, we can assume that the number of both tau molecules and their binding sites are at a constant level during an FDAP experiment.
4. Transport of tau along the cellular process can be neglected during an FDAP/FRAP experiment. It has been proposed previously that tau is actively transported along the axon at rates of slow axonal transport (0.002 μm/s on average) (25,43). However, this mechanism of tau distribution seems to be very efficient only at longer distances (hundreds of micrometers) and/or timescales (hours). None of these spatiotemporal characteristics arises during an FDAP/FRAP experiment, which lasts on average several minutes and encompasses an area several tens of micrometers in diameter. Thus, diffusion through the cytosol should dominate on these scales.

   To quantitatively support the above reasoning we generalize Eq. 2 so that it accounts for the transport. Namely,

$$\frac{\partial[\mathrm{TF}]}{\partial t} = D\frac{\partial^2[\mathrm{TF}]}{\partial z^2} + v\frac{\partial[\mathrm{TF}]}{\partial z} - k^*_{\mathrm{on}}[\mathrm{TF}] + k_{\mathrm{off}}[\mathrm{TB}], \tag{12A}$$

$$\frac{\partial[\mathrm{TB}]}{\partial t} = k^*_{\mathrm{on}}[\mathrm{TF}] - k_{\mathrm{off}}[\mathrm{TB}], \tag{12B}$$

where v denotes the average velocity of slow axonal transport. Our task is to find a limit on the parameters of the system at which transport processes can be neglected while performing FDAP/FRAP. To do this, let us calculate fluxes of activated tau proteins through two arbitrary planes located perpendicular to the cell process and equidistant from the activation region, $\{z = \pm L\}$, $L > \sigma$, and calculate the difference between the fluxes. Mathematically, the difference can be written as $\Delta J = J_{\rightarrow} - J_{\leftarrow}$, where $J_{\rightarrow} = (\vec{J} \times \vec{n}_{\rightarrow})$, $J_{\leftarrow} = (\vec{J} \times \vec{n}_{\leftarrow})$, $\vec{J} = -D\nabla[\mathrm{TF}] + \vec{v}[\mathrm{TF}]$ is the flux, composed of a diffusive component and an advective flux, and $\vec{n}_{\rightarrow}$ and $\vec{n}_{\leftarrow}$ are normals to the planes pointing away from the activation region. Following the solution strategy described in the Supporting Material, one finds the expression for the Laplace image of the difference:

$$\Delta\overline{J} = \frac{2v[\mathrm{TF}]_{\mathrm{eq}}}{p(\mu_1/\mu_2 - 1)}(\exp(-\mu_2\sigma) - \exp(-\mu_1\sigma))\exp(\mu_1 L), \tag{14}$$

where $\mu_{1,2} = -v/2D \mp \sqrt{v^2/4D^2 + q^2}$, σ is the half-length of the activation region, and q is a parameter that depends on p, k^*_{on}, k_{off}, and D (see Supporting Material).

The transport can be neglected if $|\Delta J| \rightarrow 0$, whereas $v \neq 0$. The only condition under which this is achieved is when a dimensionless parameter $\xi = v\sigma/2D \rightarrow 0$, in other words, when the velocity of transport is much less than a critical transport velocity, $v_{\mathrm{critical}} = 2D/\sigma$. The critical transport velocity in our experiments varied from ~3.6 μm/s to ~7.2 μm/s depending on the size of the activation region. According to Scholz and Mandelkow (25) and Mercken et al. (43), tau is cotransported along with short MTs from cell bodies into axons at the average rate of 0.002 μm/s, which is much less than the critical transport velocity in our experiments, and so the transport can be neglected in the reaction-diffusion models (Eqs. 2 and 5).

5. The concentration of specific binding sites related to MTs is large relative to that of other binding sites unrelated to MTs. Tau is a multifunctional protein that interacts with many partners in neurons (44), e.g., the neural plasma membrane (45). The proportion of tau binding to these partners has not been quantified previously. Our recent data by single-molecule analysis (26) suggest that MTs are the dominant interaction partners of tau in the neuritic shaft. This justifies restricting the reaction-diffusion model to only two states of tau, free (TF) and bound to MTs (TB). Non-MT binding sites are thus neglected. This is equivalent to the assumption that the concentration of MT-specific binding sites is much higher than that of non-MT binding sites.
6. The total concentration of tau molecules does not considerably exceed the concentration of the available binding sites. Knowing whether or not the MT array is oversaturated by bound tau molecules is important for the determination of k^*_{on}. If the MT array is oversaturated, i.e., the total concentration of tau considerably exceeds that of binding sites on MTs, the kinetic model (Eq. 2) may underestimate the pseudo-on-rate due to the lack of binding possibilities for free tau. According to Butner and Kirschner (46), tau has a relatively weak affinity for MTs ($K_{\mathrm{d}} \approx 10^{-7}$ M). One can hence estimate the concentration of binding sites for tau, $[\mathrm{MT}]_{\mathrm{eq}}$, using Eq. 3:

$$K_{\mathrm{d}} = \frac{[\mathrm{TF}]_{\mathrm{eq}}[\mathrm{MT}]_{\mathrm{eq}}}{[\mathrm{TB}]_{\mathrm{eq}}} = \frac{k_{\mathrm{off}}}{k^*_{\mathrm{on}}}[\mathrm{MT}]_{\mathrm{eq}}. \tag{15}$$

Substituting the experimental values for the pseudo-on- and off-rates (Table 2, *hybrid behavior*) into Eq. 15 yields $[\mathrm{MT}]_{\mathrm{eq}} \approx 5$ μM. This value is compatible with the average concentration of tau in living cells, ~5 μM (39). Note that $[\mathrm{MT}]_{\mathrm{eq}}$ reflects the concentration of binding sites for PAGFP-tau but not of the endogenous tau. This means that MTs are not oversaturated even by bringing in the exogenous PAGFP-tau. Hence, $[\mathrm{TF}]_{\mathrm{eq}} + [\mathrm{TB}]_{\mathrm{eq}} \leq [\mathrm{MT}]_{\mathrm{eq}}$.

The topology of MT arrays and consequences for the interpretation of FDAP/FRAP data

This study represents a rigorous reaction-diffusion theory for FDAP/FRAP analysis of the tau-MT interaction in processes of living cells that accounts for several considerable omissions in previous studies (14,15,17). First, the presented formalism bridges the gap between techniques based on ensemble measurements (such as FDAP, FRAP, and FCS) and single-molecule approaches at high spatiotemporal resolution. This is achieved by explicitly considering the fine structure of the MT array in the reaction-diffusion equations. The mean spacing between MTs in the array ($R_{\mathrm{MT\text{-}MT}}$) is greater than the radius of an MT ($R_{\mathrm{MT}} << R_{\mathrm{MT\text{-}MT}}$ for PC12 cells). The binding sites for MAPs on MTs are not homogenously distributed over the cellular process but are clustered on the MT filaments. To our knowledge, full analytical solutions to mathematical equations describing this heterogeneous reaction-diffusion problem have not yet been published. Coarse-grain averaging, however, allows extrapolation of the analytical solutions for the homogenous case to the heterogeneous one. In EMA (34,35), the volume fill factor of reactive obstacles, φ, is introduced to reduce the reaction-diffusion equations of

the inhomogeneous problem to a form resembling that of the homogenous one with three, now effective, parameters, D, k^*_{on}, and k_{off}. The orientation of the biopolymer network also plays an important role in defining the effective diffusion constant. We have shown via Monte Carlo simulations that the longitudinal diffusion along the array of parallel MTs remains unaffected even for quite large values of φ (Fig. 3). The true rate constants for binding ($\overline{k}^*_{on}$) and dissociation ($\overline{k}_{off}$) are then related to the effective ones through the volume fill factor, namely, $k^*_{on} = \varphi\overline{k}^*_{on}$ and $k_{off} = \varphi\overline{k}_{off}$, whereas the equilibrium constant is independent of the volume fill factor, $K_{eq} = \overline{k}_{on}/\overline{k}_{off} = k_{on}/k_{off}$. The apparent association and dwell times of tau in the MT array, as inferred by interpreting FDAP transients in terms of the reaction-diffusion model with homogeneously distributed binding sites, are $1/\varphi$ times longer than the actual dwell times related to a single MT. Second, our experimental values for the dwell time ($\leq$100 ms) of tau on a single MT in processes of living PC12 cells compare well with those recently obtained by single molecule analysis in processes of living PC12 cells (~40 ms), as well as in cultured cortical neurons (26). This result, however, does not disprove the much longer dwell time of ~4 s revealed by FRAP in axons of living neurons (14). Indeed, without considering the fine structure of the MT array, the FDAP/FRAP analysis estimates a dwell time of tau on the MT array as a whole. Once the fine MT structure is taken into account, the FDAP/FRAP analysis increases its resolution to measure a dwell time of tau on a single MT filament. Interestingly, this appears to be an accurate tool to estimate the volume fill factor of MTs in processes of living neuronal cells, since $k_{off} = \varphi\overline{k}_{off}$. The value $\varphi_{max} \approx 0.013$, which was roughly computed based on a regular shape of the cross section of the process and an optimal arrangement of MTs, is thus a good estimate of $\varphi \approx 0.01$ based on a combination of the FDAP/FRAP and single-molecule data. Third, we analyzed a more complex case of tau distribution along the cellular process, namely, the diffusion of bound tau. Our results show that in contrast to in vitro data, this phenomenon is rather negligible in living cells (36). We speculate that there are two possible explanations for this discrepancy. On the one hand, the diffusion of bound tau may not occur in living cells due to its rapid on-off kinetics, i.e., a dwell time of tau on single MTs that is simply too short. On the other hand, Hinrichs et al. (36) used labeling of cysteine residues at positions 291 and 322, which are located directly in the repeat region of tau. This might have encouraged conformations that allow the diffusion of tau in the bound state. Our findings are also of interest methodologically. The simplified solutions for pure and effective diffusion are still applicable (see Supporting Material and Fig. S2). As D_B increased and approached D_F, the parametric region that was not assigned to any of the simplified solutions was reduced and nearly vanished. We also found a parametric region where the diffusing-bound-state model could be formally well described by the first scenario without diffusion in the bound state. If the kinetic parameters were in this particular domain, the respective diffusion constants of the free and bound proteins could not be independently extracted from the FDAP transients. It seems impossible that multicomponent reaction-diffusion systems with fast and slow components can provide independent estimates for the diffusion constants under certain constraints on the reaction rates, although the reaction rates themselves can still be independently extracted. The region was quite large at small values of D_B and also vanished as D_B approached D_F (see Fig. S2). Finally, we have demonstrated that the transport of tau along cellular processes can be neglected while performing an FDAP/FRAP experiment. Although this appears to be a very efficient mechanism of translocation of tau toward growth cones, on moderate spatiotemporal scales (several tens of micrometers and several minutes), diffusion through the cytosol prevails.

The rapid dynamics of tau and its effect on MT regulation

Our study indicates that the dwell time of tau in an MT array, as it exists in an axon, is ~100-fold shorter than previously estimated. What are the consequences of such a short interaction with respect to a mechanistic understanding of the role of tau in regulating the axonal MT dynamics? In cell-free assays, tau suppresses the MT dynamics already at concentrations that are 10- to 20-fold lower than the physiological tau/tubulin ratio (12), which might indicate that microtubules react in a very sensitive manner to the presence of tau. Let us assume that the affinity of tau for MTs does not depend on a position on each particular MT, i.e., that it is identical for MT tips and the remaining parts. A recent study (47) on the kinetics of MT assembly revealed that the association and dissociation rates of tubulin to/from MTs both depend on the free tubulin concentration and are nearly equal to each other at all free tubulin concentrations. These rates also turned out to be higher by an order of magnitude than previously thought. According to this study, the MT assembly is hypersensitive to small changes in the tubulin off-rate, namely, a 10-fold increase in the net growth rate of an MT can be achieved by increasing the lifetime of tubulin in the GTP cap by a factor of 2. Under physiological concentrations, the average lifetime of a tubulin dimer in the GTP cap of an MT is ~1 ms (48). Hence, even a dwell time of tau on MTs that is only several tens of milliseconds ($\leq$100 ms in our study) would be enough to suppress the tubulin off-rate. Permanent or long-lived (~4 s, as in Konzack et al. (14)) binding of tau to MTs is simply not required to fulfill this function. Binding to the rest of MTs probably serves other functions, such as maintaining the MT-MT distance (49) and protecting MTs from severing enzymes like katanin (50).

The rapid dynamics of tau and its effect on the axonal transport

In vitro studies (6,51) have provided evidence that binding of tau to MTs affects the mobility of kinesin, suggesting that tau inhibits fast axonal transport. However, results from these studies are not consistent with in vivo experiments (9), where even a high excess of tau did not interfere with fast axonal transport. Thus, it seems surprising that tau, despite being up to ~98% bound to MTs, does not affect the axonal vesicle transport rates. The solution to this puzzle, we think, is that the assumption that axonal MTs are decorated by long interacting tau proteins is wrong (see, e.g.,Dixit et al. (6)). If the true dwell time of tau on a MT was several seconds, as suggested by the homogenous reaction-diffusion model, one would expect hindrance of the active movement of motorproteins progressing at an average velocity of ~1 μm/s (52). Given the total concentration of tau in neuronal cells, ~5 μM (39), and the average ratio of bound tau molecules, $[\mathrm{TB}]_{\mathrm{eq}} \approx 98\%$, the average distance between the two closest tau molecules bound to the same MT, $<l>$, can be estimated using the formula $<l>^2 = S_{\mathrm{MT}}/N_{\mathrm{tau}}$, where $<l>^2$ is the average minimal area per bound tau molecule, S_{MT} is the total area of the MT surface, and N_{tau} is the total number of bound tau molecules. For a cellular process of radius $R = 0.5$ μm filled with $N_{\mathrm{MT}} = 60$ parallel MTs, each of radius $R_{\mathrm{MT}} =$ 12.5 nm (20), we come up with $<l> \approx 45$ nm. This implies that a processing kinesin molecule would encounter ~170 bound tau molecules within the dwell time (~7.7 s) suggested by the homogeneous reaction-diffusion model. Since the true dwell time of tau on MTs is shorter by two orders of magnitude, the apparent paradox is resolved. On average, bound tau molecules dissociate before being encountered by kinesins; the fast dissociation in turn is compensated by the high association rate of tau to MTs. Almost constant binding of tau does not contradict the high on- and off-rates.

SUPPORTING MATERIAL

Two figures and additional supplemental information are available at http://www.biophysj.org/biophysj/supplemental/S0006-3495(14)00955-2.

We thank Vanessa Herkenhoff for technical help and the reviewers for their very helpful comments.

This work was supported by the Bundesministerium für Bildung und Forschung (KMU-innovativ-7 to R.B.) and the Sonderforschungsbereich (SFB944, Z-project). W.J. holds a Niedersachsen-Professur awarded by the State of Lower Saxony, Germany.

SUPPORTING CITATIONS

References (53–59) appear in the Supporting Material.

REFERENCES

1. Hirokawa, N., and R. Takemura. 2005. Molecular motors and mechanisms of directional transport in neurons. *Nat. Rev. Neurosci.* 6:201–214.
2. Hirokawa, N. 1994. Microtubule organization and dynamics dependent on microtubule-associated proteins. *Curr. Opin. Cell Biol.* 6:74–81.
3. Chen, J., Y. Kanai, …, N. Hirokawa. 1992. Projection domains of MAP2 and tau determine spacings between microtubules in dendrites and axons. *Nature.* 360:674–677.
4. Seeger, M. A., and S. E. Rice. 2010. Microtubule-associated protein-like binding of the kinesin-1 tail to microtubules. *J. Biol. Chem.* 285:8155–8162.
5. Seitz, A., H. Kojima, …, E. Mandelkow. 2002. Single-molecule investigation of the interference between kinesin, tau and MAP2c. *EMBO J.* 21:4896–4905.
6. Dixit, R., J. L. Ross, …, E. L. F. Holzbaur. 2008. Differential regulation of dynein and kinesin motor proteins by tau. *Science.* 319:1086–1089.
7. Ebneth, A., R. Godemann, …, E. Mandelkow. 1998. Overexpression of tau protein inhibits kinesin-dependent trafficking of vesicles, mitochondria, and endoplasmic reticulum: implications for Alzheimer's disease. *J. Cell Biol.* 143:777–794.
8. Morfini, G., G. Pigino, and S. T. Brady. 2007. Approaches to kinesin-1 phosphorylation. *Methods Mol. Biol.* 392:51–69.
9. Yuan, A., A. Kumar, …, R. A. Nixon. 2008. Axonal transport rates in vivo are unaffected by tau deletion or overexpression in mice. *J. Neurosci.* 28:1682–1687.
10. McVicker, D. P., L. R. Chrin, and C. L. Berger. 2011. The nucleotide-binding state of microtubules modulates kinesin processivity and the ability of Tau to inhibit kinesin-mediated transport. *J. Biol. Chem.* 286:42873–42880.
11. Mitchison, T., and M. Kirschner. 1984. Dynamic instability of microtubule growth. *Nature.* 312:237–242.
12. Panda, D., B. L. Goode, …, L. Wilson. 1995. Kinetic stabilization of microtubule dynamics at steady state by tau and microtubule-binding domains of tau. *Biochemistry.* 34:11117–11127.
13. Bunker, J. M., L. Wilson, …, S. C. Feinstein. 2004. Modulation of microtubule dynamics by tau in living cells: implications for development and neurodegeneration. *Mol. Biol. Cell.* 15:2720–2728.
14. Konzack, S., E. Thies, …, E. Mandelkow. 2007. Swimming against the tide: mobility of the microtubule-associated protein tau in neurons. *J. Neurosci.* 27:9916–9927.
15. Breuzard, G., P. Hubert, …, V. Peyrot. 2013. Molecular mechanisms of Tau binding to microtubules and its role in microtubule dynamics in live cells. *J. Cell Sci.* 126:2810–2819.
16. Samsonov, A., J.-Z. Yu, …, S. V. Popov. 2004. Tau interaction with microtubules in vivo. *J. Cell Sci.* 117:6129–6141.
17. Weissmann, C., H.-J. Reyher, …, R. Brandt. 2009. Microtubule binding and trapping at the tip of neurites regulate tau motion in living neurons. *Traffic.* 10:1655–1668.
18. Sprague, B. L., R. L. Pego, …, J. G. McNally. 2004. Analysis of binding reactions by fluorescence recovery after photobleaching. *Biophys. J.* 86:3473–3495.
19. Michelman-Ribeiro, A., D. Mazza, …, J. G. McNally. 2009. Direct measurement of association and dissociation rates of DNA binding in live cells by fluorescence correlation spectroscopy. *Biophys. J.* 97:337–346.
20. Jacobs, J. R., and J. K. Stevens. 1986. Changes in the organization of the neuritic cytoskeleton during nerve growth factor-activated differentiation of PC12 cells: a serial electron microscopic study of the development and control of neurite shape. *J. Cell Biol.* 103:895–906.
21. Crank, J. 1975. The Mathematics of Diffusion. Oxford University Press, New York.
22. Junge, W., and A. Polle. 1986. Theory of proton flow along appressed thylakoid membranes under both non-stationary and stationary conditions. *Biochim. Biophys. Acta.* 848:265–273.
23. Polle, A., and W. Junge. 1989. Proton diffusion along the membrane surface of thylakoids is not enhanced over that in bulk water. *Biophys. J.* 56:27–31.

24. Junge, W., and S. McLaughlin. 1987. The role of fixed and mobile buffers in the kinetics of proton movement. *Biochim. Biophys. Acta.* 890:1–5.

25. Scholz, T., and E. Mandelkow. 2014. Transport and diffusion of Tau protein in neurons. *Cell. Mol. Life Sci.* 71:3139–3150. http://dx.doi.org/10.1007/s00018–014–1610–7.

26. Janning, D., M. Igaev, …, R. Brandt. 2014. Single molecule tracking of tau reveals fast kiss-and-hop interaction with microtubules in living neurons. *Mol. Biol. Cell.* http://dx.doi.org/10.1091/mbc.E14–06–1099.

27. Gauthier-Kemper, A., C. Weissmann, …, R. Brandt. 2011. The frontotemporal dementia mutation R406W blocks tau's interaction with the membrane in an annexin A2-dependent manner. *J. Cell Biol.* 192:647–661.

28. Gauthier-Kemper, A., C. Weissmann, …, R. Brandt. 2012. Monitoring cytoskeletal dynamics in living neurons using fluorescence photoactivation. *Methods Enzymol.* 505:3–21.

29. Fath, T., J. Eidenmüller, and R. Brandt. 2002. Tau-mediated cytotoxicity in a pseudohyperphosphorylation model of Alzheimer's disease. *J. Neurosci.* 22:9733–9741.

30. Chatterjee, A. P. 2011. Tracer diffusion in fibre networks: the impact of spatial fluctuations in the fibre distribution. *J. Phys. Condens. Matter.* 23:375103.

31. Jiao, Y., and S. Torquato. 2012. Quantitative characterization of the microstructure and transport properties of biopolymer networks. *Phys. Biol.* 9:036009.

32. Keener, J. 2000. Homogenization and propagation in the bistable equation. *Physica D.* 136:1–17.

33. Runborg, O., C. Theodoropoulos, and I. G. Kevrekidis. 2002. Effective bifurcation analysis: a time-stepper-based approach. *Nonlinearity.* 15:491–511.

34. Bedeaux, D., and R. Kapral. 1983. The effective reaction rate and diffusion coefficients for a two-phase medium. *J. Chem. Phys.* 79:1783–1788.

35. Alonso, S., R. Kapral, and M. Bär. 2009. Effective medium theory for reaction rates and diffusion coefficients of heterogeneous systems. *Phys. Rev. Lett.* 102:238302.

36. Hinrichs, M. H., A. Jalal, …, T. Scholz. 2012. Tau protein diffuses along the microtubule lattice. *J. Biol. Chem.* 287:38559–38568.

37. Mazza, D., A. Abernathy, …, J. G. McNally. 2012. A benchmark for chromatin binding measurements in live cells. *Nucleic Acids Res.* 40:e119.

38. Gustke, N., B. Trinczek, …, E. Mandelkow. 1994. Domains of tau protein and interactions with microtubules. *Biochemistry.* 33:9511–9522.

39. Brandt, R., and G. Lee. 1993. Functional organization of microtubule-associated protein tau. Identification of regions which affect microtubule growth, nucleation, and bundle formation in vitro. *J. Biol. Chem.* 268:3414–3419.

40. Black, M. M., T. Slaughter, …, I. Fischer. 1996. Tau is enriched on dynamic microtubules in the distal region of growing axons. *J. Neurosci.* 16:3601–3619.

41. Kempf, M., A. Clement, …, R. Brandt. 1996. Tau binds to the distal axon early in development of polarity in a microtubule- and microfilament-dependent manner. *J. Neurosci.* 16:5583–5592.

42. Litman, P., J. Barg, …, I. Ginzburg. 1993. Subcellular localization of tau mRNA in differentiating neuronal cell culture: implications for neuronal polarity. *Neuron.* 10:627–638.

43. Mercken, M., I. Fischer, …, R. A. Nixon. 1995. Three distinct axonal transport rates for tau, tubulin, and other microtubule-associated proteins: evidence for dynamic interactions of tau with microtubules in vivo. *J. Neurosci.* 15:8259–8267.

44. Morris, M., S. Maeda, …, L. Mucke. 2011. The many faces of tau. *Neuron.* 70:410–426.

45. Brandt, R., J. Léger, and G. Lee. 1995. Interaction of tau with the neural plasma membrane mediated by tau's amino-terminal projection domain. *J. Cell Biol.* 131:1327–1340.

46. Butner, K. A., and M. W. Kirschner. 1991. Tau protein binds to microtubules through a flexible array of distributed weak sites. *J. Cell Biol.* 115:717–730.

47. Gardner, M. K., B. D. Charlebois, …, D. J. Odde. 2011. Rapid microtubule self-assembly kinetics. *Cell.* 146:582–592.

48. Brandt, R., and G. Lee. 1993. The balance between tau protein's microtubule growth and nucleation activities: implications for the formation of axonal microtubules. *J. Neurochem.* 61:997–1005.

49. Rosenberg, K. J., J. L. Ross, …, J. Israelachvili. 2008. Complementary dimerization of microtubule-associated tau protein: implications for microtubule bundling and tau-mediated pathogenesis. *Proc. Natl. Acad. Sci. USA.* 105:7445–7450.

50. Qiang, L., W. Yu, …, P. W. Baas. 2006. Tau protects microtubules in the axon from severing by katanin. *J. Neurosci.* 26:3120–3129.

51. Tarhan, M. C., Y. Orazov, …, H. Fujita. 2013. Biosensing MAPs as "roadblocks": kinesin-based functional analysis of tau protein isoforms and mutants using suspended microtubules (sMTs). *Lab Chip.* 13:3217–3224.

52. Roy, S., M. J. Winton, …, V. M.-Y. Lee. 2007. Rapid and intermittent cotransport of slow component-b proteins. *J. Neurosci.* 27:3131–3138.

53. Hecht, F. 2012. New development in freefem++. *J. Numer. Math.* 20:251–265.

54. Oliphant, T. E. 2007. Python for scientific computing. *Comput. Sci. Eng.* 9:10–20.

55. Valsa, J., and L. Brančik. 1998. Approximate formulae for numerical inversion of Laplace transforms. *Int. J. Numer. Model. Electron. Networks. Devices Fields.* 11:153–166.

56. Bates, D. M., and D. G. Watts. 1988. Nonlinear Regression Analysis and Its Applications. John Wiley & Sons, Hoboken, NJ.

57. Moya-Cessa, H. M., and F. Soto-Eguibar. 2011. Differential Equations: An Operational Approach. Rinton Press, Princeton, NJ.

58. Lubachevsky, B., and R. Graham. 1997. Curved hexagonal packings of equal disks in a circle. *Discrete Comput. Geom.* 194:179–194.

59. Graham, R. L., B. D. Lubachevsky, …, P. R. J. Östergård. 1998. Dense packings of congruent circles in a circle. *Discrete Math.* 181:139–154.